



Machine learning enabled compact flexible full ground UWB antenna for wearable applications

Alladi Praveena¹ , Govindaswamy Umamaheswari¹, Jayant Kumar Rai² and Pinku Ranjan²

¹Department of Electronics and Communication Engineering, PSG College of Technology, Coimbatore, India and

²Department of Electrical and Electronics Engineering, ABV Indian Institute of Information Technology and Management, Gwalior, India

Research Paper

Cite this article: Praveena A, Umamaheswari G, Rai JK, Ranjan P (2024) Machine learning enabled compact flexible full ground UWB antenna for wearable applications. *International Journal of Microwave and Wireless Technologies*, 1–13. <https://doi.org/10.1017/S1759078724000837>

Received: 16 February 2024

Revised: 13 August 2024

Accepted: 18 August 2024

Keywords:

flexible antenna; machine learning; Poly-dimethyl siloxane (PDMS); wearable applications; ultra-wideband

Corresponding author: Pinku Ranjan;

Email: pinkuranjan@iiitm.ac.in

Abstract

This work introduces a novel compact ultra-wideband (UWB) antenna designed for wearable applications, employing a bioinspired structure and machine learning (ML) techniques to achieve exceptional performance in the 3.10–10.42 GHz range. The antenna is fabricated by positioning conductive fabric on a polydimethylsiloxane polymer of 1 mm thickness to augment high flexibility and durability. Additionally, it pioneers integrating a complete ground plane to mitigate back radiation toward the human body, presenting a compact ($35.5 \times 30.5 \times 1 \text{ mm}^3$) UWB antenna design compliant with IEEE 802.15.6 standards. The design methodology includes using bandwidth enhancement techniques such as chamfering edges, slots, and adding stubs in the feed, along with applying ML to optimize the antenna's dimensions for desired return loss characteristics. The proposed antenna demonstrates exceptional resilience to human body loading and physical deformation. The simulation and measurement results have good agreement. The K-nearest neighbour method beat the other ML algorithms maximum accuracy of 99.62% to predict the S_{11} . According to the author's best knowledge, this is the first compact UWB antenna with full ground specified by IEEE.802.15.6 with ML reported.

Introduction

In recent years, there has been a significant increase in interest in wireless body area networks (WBAN), since advancements in wireless communication have led to the development of cutting-edge technologies like 5G and the internet of things. These technologies will bring new experiences to industry and society. Furthermore, it will lead to a significant change in how we live in this world. Integrating WBAN with these technologies provides connectivity between everything and anything [1–3]. WBAN deals with several critical applications, such as disaster management services, care for the elderly and impoverished children, sports, internet of military things, health monitoring, emergency rescue services, and so on [1–6]. In the Federal Communication Commission (FCC), the U.S., in 2002, the unlicensed ultra-wideband (UWB) applications were assigned a range of frequencies from 3.1 to 10.6 GHz. Based on the most recent IEEE 802.15.6 WBAN standard, UWB technology has been expanded into the application of WBAN [7–11]. It is a high-speed data transmission method that is resistant to multipath interference and jamming due to its low chance of detection [12, 13]. In a WBAN system, the UWB technology is a suitable candidate to reduce power spectrum density, resulting in longer battery life and lower electromagnetic exposure [14–18]. WBAN connectivity is offered using small, flexible, lightweight UWB antennas that are unobtrusive to the user [11,12]. Antennas worn ON or OFF the body are crucial for establishing contact with certain devices in WBAN networks [1, 18]. According to the literature, most wearable antennas operating in the UWB band use a partial or faulty ground plane to increase bandwidth [19]. However, because of the high permittivity and lossy nature of the layers of human flesh underneath it, antennas without a complete ground plane are not appropriate for wearable applications [20]. This affects the antenna's performance and raises the specific absorption rate (SAR). Most wearable antennas were prototyped using textile materials to increase flexibility, even though newer UWB antenna designs with a complete ground plane attempt to overcome these problems. However, after a few washes, they become extremely deformed and are sensitive to moisture and humidity. As a result, they cannot be used in severe environments like those seen in wearable applications. On the other hand, a few researchers [15, 21–26] reported durable UWB antennas with full planes, which may occupy more space, or multilayered antennas that may not fit into portable devices.

In this paper, a compact antenna for WBAN applications in the 3.1–10.42 GHz frequency band is designed. The proposed antenna is prototyped with a conductive fabric, on a 1 mm thick

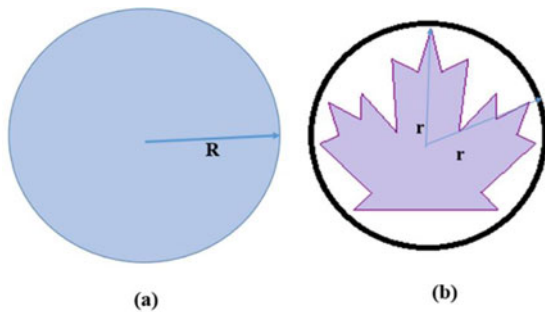


Figure 1. (a) Circular patch with radius “ R ” = 10 mm (b) maple leaf patch with maximum edge length “ r ” of 10 mm from its center.

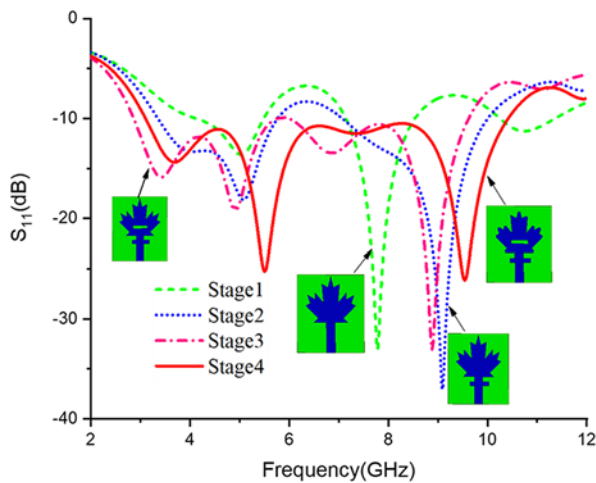


Figure 2. Evolutionary stages and their return loss characteristics.

Table 1. Details of the evolutionary stages and reflection characteristics

Evolutionary stage	No. of bands	Frequency range (GHz)	Bandwidth (GHz)
1	3	4.12–5.48, 7.15–8.53, 10.25–11.36	3.85
2	2	3.38–5.74, 7.12–9.97	5.21
3	2	3.13–5.67, 6.08–9.60	6.06
4	1	3.1–10.42	7.32

polydimethylsiloxane (PDMS) material that is biocompatible, highly elastic, heat resistant, watertight, and optically transparent (90%) [19, 21, 27, 28]. A full ground plane is maintained to minimize the back radiation and obtain low SAR values. However, an antenna with a thin substrate and full ground plane leads to a narrow bandwidth. To overcome this, a bioinspired maple leaf structure with serrated edges is chosen due to its multiband resonating capabilities with wider bandwidth. Further, the bandwidth enhancement techniques of chamfering edges, slots, and adding stubs in the feed are employed to achieve an UWB frequency range. A machine learning (ML) approach is used to fix the final dimensions of the antenna with desired return loss characteristics.

Thus, the proposed antenna design has the following attractive characteristics:

- 1) It has a novel and compact structure with a full-ground plane that resonates at the UWB frequency range.
- 2) It has a boresight radiation pattern, as required for WBAN applications.
- 3) It exhibits significantly lower SAR values than the FCC standards due to employing a full ground plane with highly conductive fabric.
- 4) It demonstrates high flexibility due to the integration of a thin layer of inherently flexible PDMS with conductive fabric.
- 5) It has a reliable performance under free space and on body conditions by maintaining 7.32 GHz and 9.8 GHz bandwidth, respectively, for $S_{11} < -10$ dB.

Antenna configuration and prototype

Modelling and evolutionary stages of the proposed antenna

The initiation of the proposed antenna begins with a circular patch with a radius (r) of 10 mm, which is considered the initiator in this work, as seen in Fig. 1(a). The equations (1–4) adapted from reference [15] are used to calculate the r to achieve a lower edge frequency (LEF) of around 3 GHz. The maple leaf, resembling an open hand with serrated edges (Fig. 1(b)), has a maximum edge length from its center of 10 mm. The initiator’s area, calculated using equation (2) for the area of a circle, is 314.2 mm². However, through measurements with the high-frequency structure simulator (HFSS), the resultant maple leaf shape is found to have an area of 239.9 mm², indicating a 14% reduction compared to the initiator. This reduction influences the LEF; an expected LEF of 3.2 GHz is calculated with the resultant area equations (3) and (4).

$$f_{lower} = \frac{0.24 \times 300}{\left(D + G + \left(\frac{D}{2\pi}\right)\right) \times K} \text{ (GHz)} \quad (1)$$

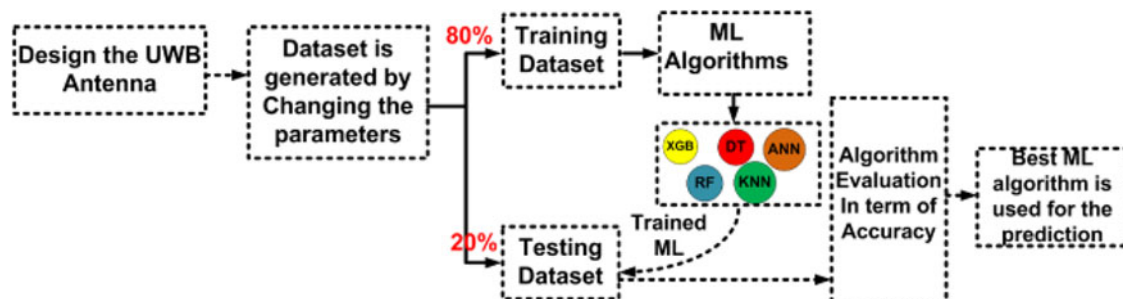


Figure 3. Flow chart of Machine Learning in the proposed UWB antenna.

$$A = \pi r^2 \tag{2}$$

$$f_r \text{ (GHz)} = \frac{300}{\varphi \sqrt{\epsilon_{eff}}} \tag{3}$$

$$\epsilon_{eff} \approx \frac{\epsilon_r + 1}{2} \tag{4}$$

The symbol “*D*” corresponds to the millimeter measurement of the circle’s diameter, the gap, expressed in millimeters, between the ground plane and the radiating patch is denoted by the letter “*G*.” “*A*” is the area of a circle. φ represents the patch’s perimeter, while ϵ_r stands for the substrate’s dielectric constant, f_r expresses the resonant frequency, and the variable k considers the influence of the substrate’s dielectric permittivity, with its value specified as 1.15 [15].

In stage 1, the patch is modified to the maple leaf structure, which resembles an open hand with serrated edges and has a maximum edge length from its center of 10 mm, which enables multiple resonating modes and results in multiple frequency bands and a total impedance bandwidth of 3.85 GHz. In stage 2, a rectangular stub is perpendicularly added to the feed line, which increases the electrical length of the antenna and results in a bandwidth of

5.21 GHz. A rectangular slot is etched in the center of the patch in stage 3, and the antenna resonates with an increased bandwidth of 6.06 GHz. Further, to tune the frequency of operation and improve the return loss (< -10 dB) for the entire UWB band, the edges of the maple leaf structure are chamfered [24]. A change in resonating modes occurred, and the increment in bandwidth was due to the chamfering of the corners, which resulted in an impedance bandwidth of 7.32 GHz. An optimization process was pursued in Ansys HFSS version 2022 to fix the dimensions and position of the slot, stub, and chamfering length. The evolution of the modified maple leaf full ground (MFG) antenna and its reflection characteristics are shown in Fig. 2. Table 1 details the frequency range, number of bands, and impedance bandwidth obtained at each evolutionary stage.

Optimization of the proposed antenna through ML

The final structure and optimal dimensions of the MFG antenna are obtained after the optimization of the antenna dimensions using ML algorithms. Figure 3 illustrates the proposed antenna’s ML flow chart. The proposed UWB antenna is designed using HFSS software. A large amount of data is required to apply the ML algorithms for the proposed antenna [29–38]. The dataset is prepared by varying the various parameters of the UWB antenna. In total, there are 4,50,451 datasets created. The whole dataset is distributed into training and testing datasets. Eighty percent of the dataset is used to train the ML algorithms, and the remaining 20% is used for testing the trained ML models. In this work, five ML algorithms, extreme gradient boosting (XGB), artificial neural network (ANN), decision tree (DT), K-nearest neighbour (KNN), and random forest (RF), are used [34–42]. Table 2 represents the ML algorithms’ mean

Table 2. MSE, MAE, and R^2 score of ML algorithms

ML algorithms	XGB	ANN	DT	KNN	RF
MSE	0.355	0.4913	0.166	0.0455	0.086
MAE	0.310	0.3852	0.106	0.0541	0.111
R^2 score	0.9706	0.9594	0.9862	0.9962	0.9928

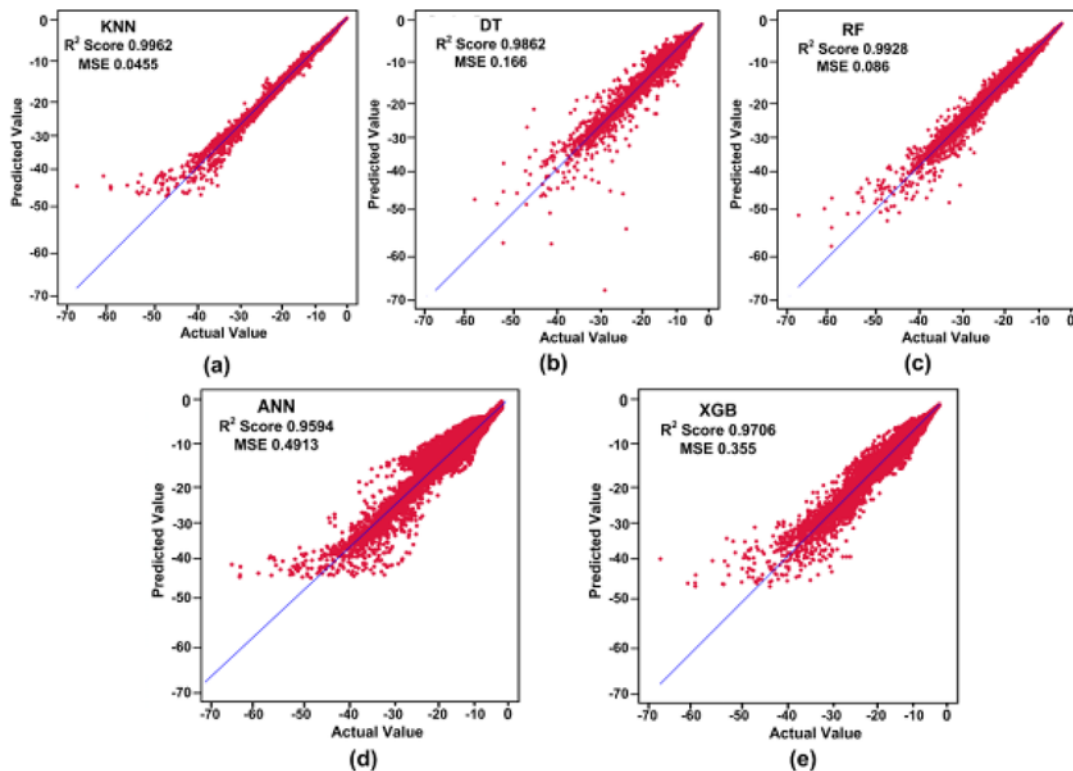


Figure 4. Actual and predicted values of ML algorithms.

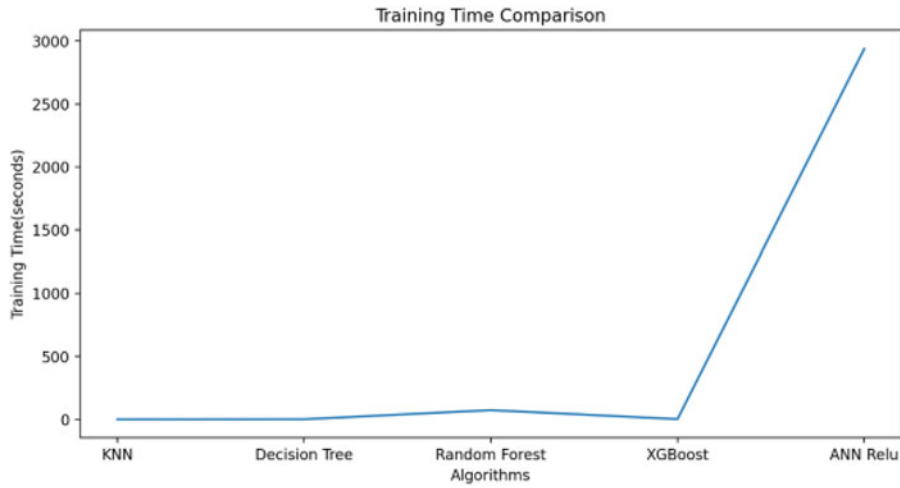


Figure 5. Training time of ML algorithms.

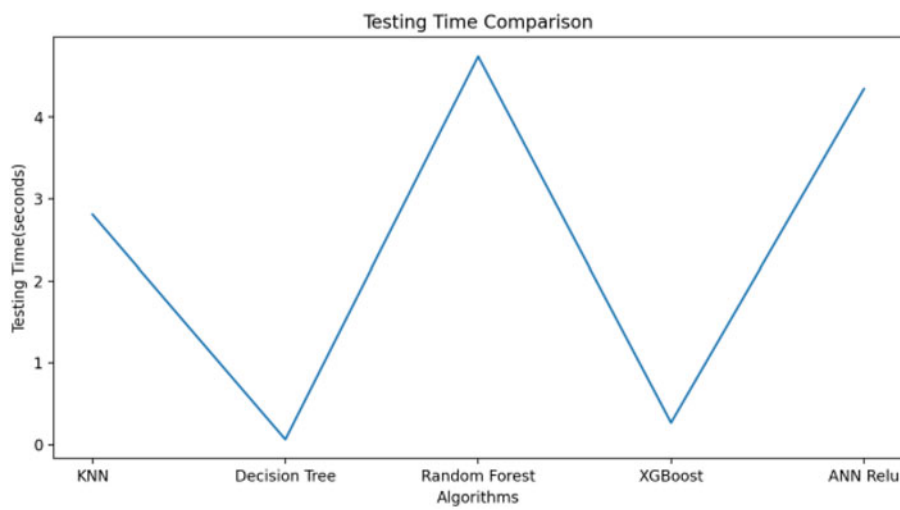


Figure 6. Testing time of ML algorithms.

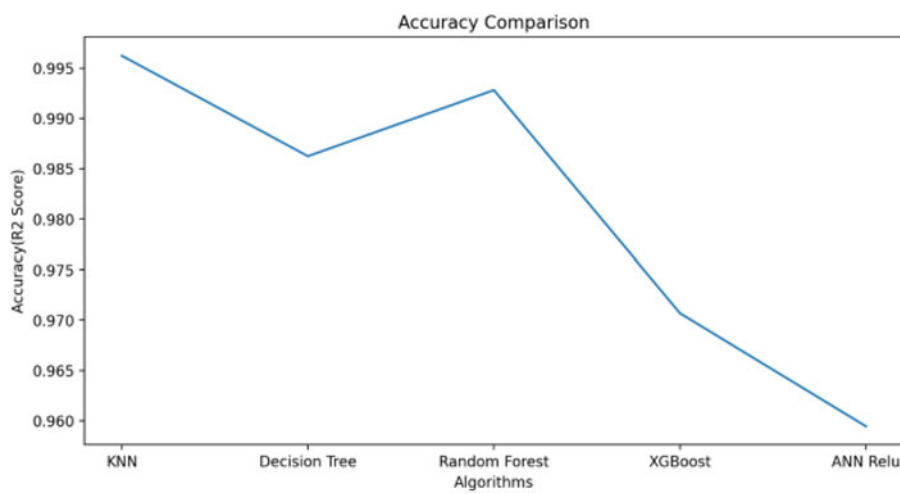


Figure 7. Accuracy of ML algorithms.

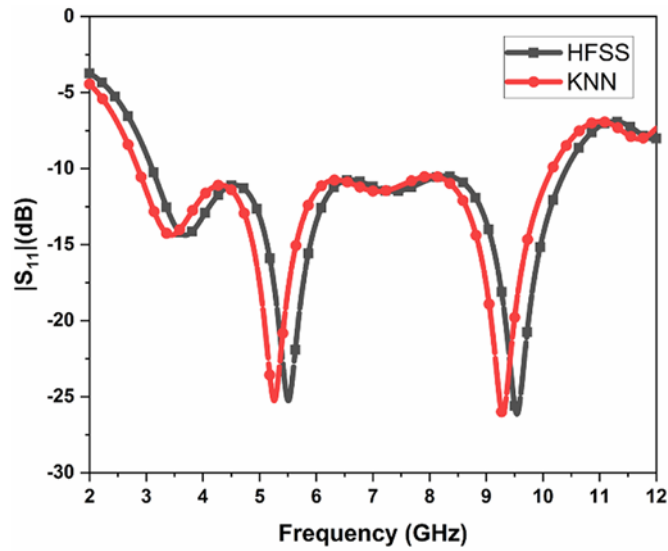


Figure 8. Comparison of KNN ML with HFSS.

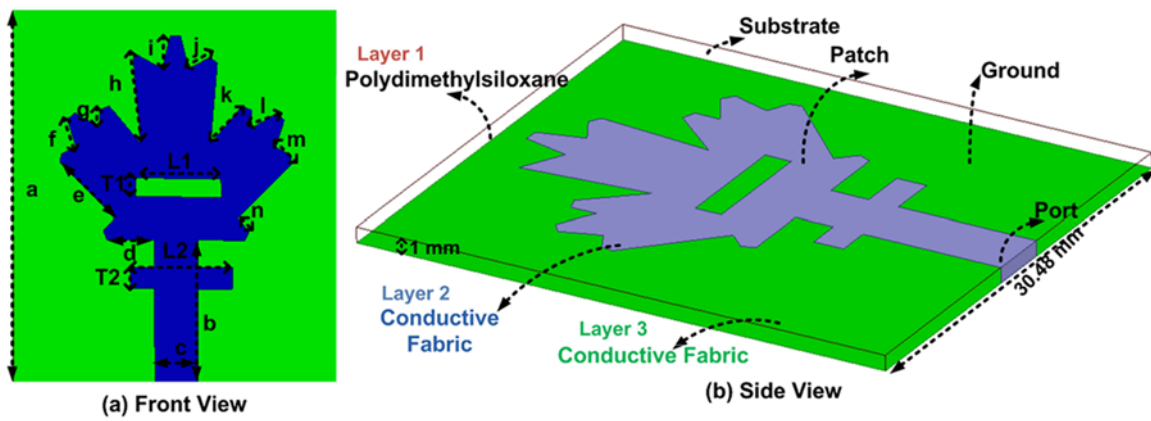


Figure 9. Dimension (in mm) (a =35.56, b =13.79, c =4.06, d =5.59, e =7.9, f =3.9, g =3, h =8.5, i =5.1, j =3, k =5.9, l =3.9, m =2.2, n =2.7).

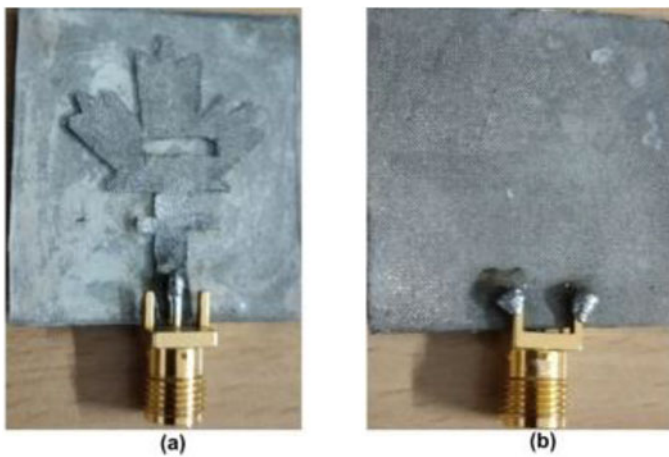


Figure 10. Prototype of the UWB antenna (a) front view and (b) rear view.

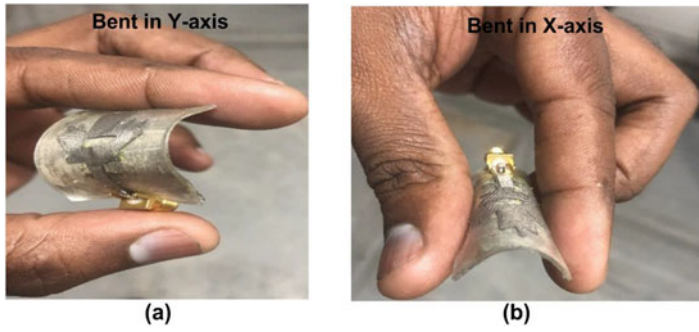


Figure 11. Flexibility of the UWB antenna (a) bent in the Y (b) X-axis.

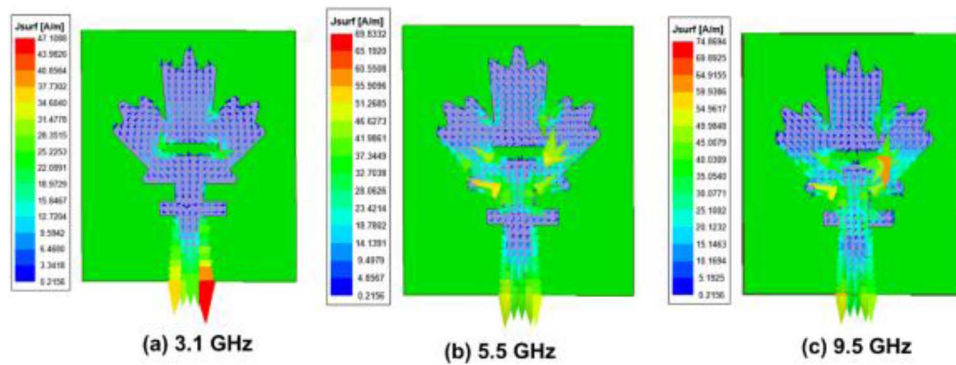


Figure 12. Surface current distribution at 3.1, 5.5, and 9.5 GHz.

Table 3. Dielectric properties of human tissue layers at various frequencies

Dielectric values at different frequencies		Human tissue layer and thickness			
		Skin (2 mm)	Fat (5 mm)	Muscle (10 mm)	Bone (10 mm)
3.8 GHz	Dielectric constant ϵ_r	36.753	5.1444	51.072	10.635
	Loss tangent δ (S/m)	0.28451	0.15792	0.26189	0.3033
7.5 GHz	Dielectric constant ϵ_r	33.638	4.8044	46.182	8.9762
	Loss tangent δ (S/m)	0.37847	0.20356	0.36955	0.41712
10 GHz	Dielectric constant ϵ_r	31.29	4.6023	42.764	8.1197
	Loss tangent δ (S/m)	0.46038	0.22857	0.44666	0.47284

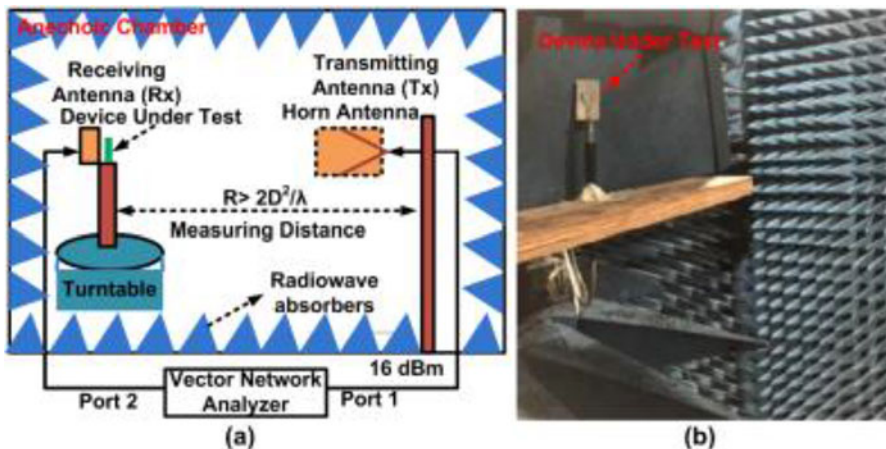


Figure 13. Anechoic chamber (a) pictorial representation, and (b) measurement setup inside the chamber.

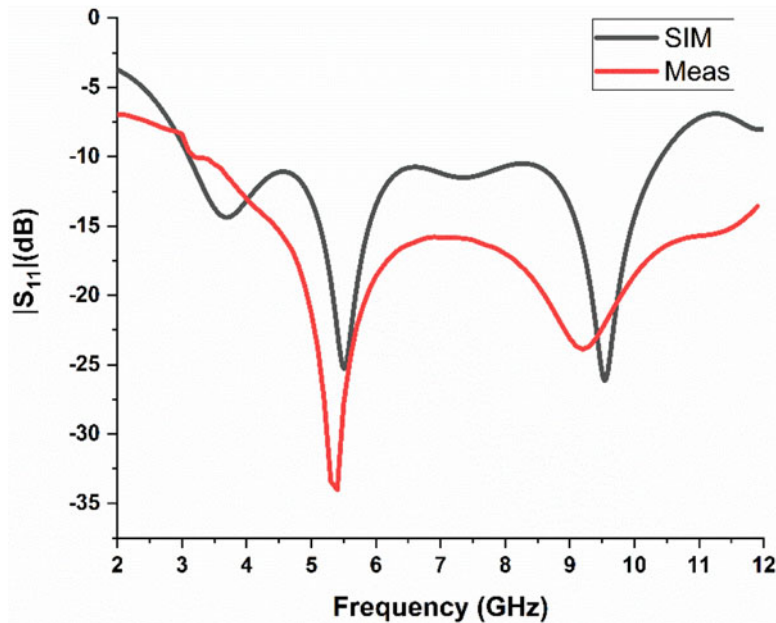


Figure 14. Comparison of the measured and simulated return loss in free space.

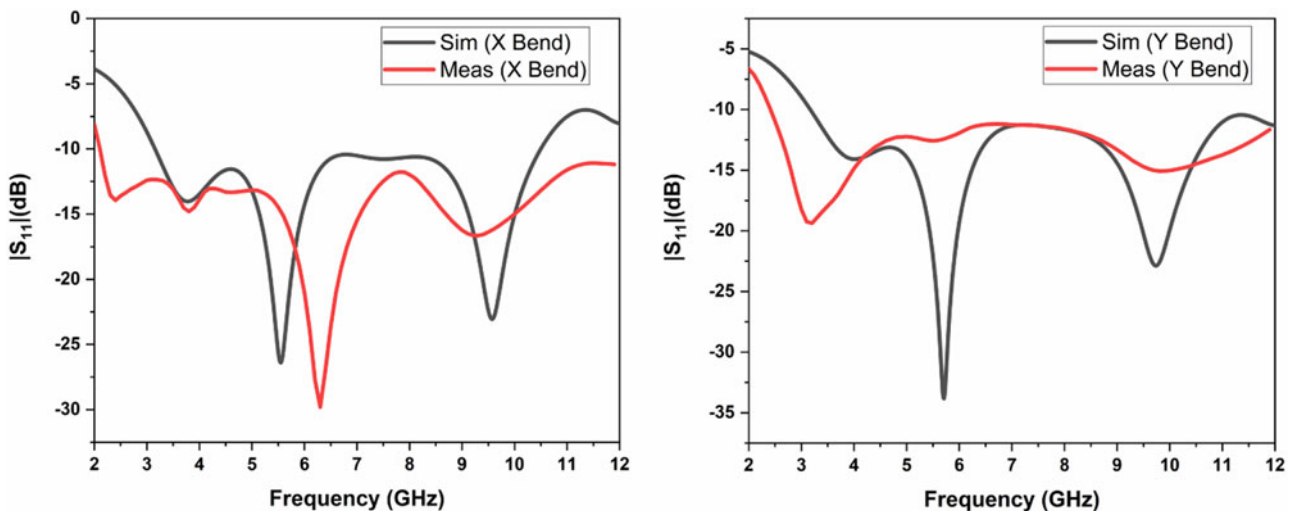


Figure 15. Comparison of measured and simulated return loss free space in X and Y axis bending.

square error (MSE), mean absolute error (MAE), and R^2 Score. Actual and predicted values of S parameters are shown in Fig. 4. R^2 Score represents the accuracy of our ML algorithms. Training time, testing time, and accuracy of various ML algorithms are represented in Figs. 5–7, respectively. From Table 2 and Fig. 7, it is seen that KNN ML algorithms achieved the highest accuracy compared to other ML algorithms. It accurately predicts the S_{11} of the proposed UWB antenna. The comparison of KNN ML with HFSS is shown in Fig. 8.

Geometry and prototyping of the proposed antenna

The proposed antenna is initially designed based on a bio-inspired maple leaf structure and further modified for desired performance characteristics, as shown in Fig. 9(a) and (b).

Bioinspired structures, such as fractal structures, are known for their compactness and increased electrical length [43–45]. The antenna has overall optimized dimensions of $35.5 \times 30.5 \times 1 \text{ mm}^3$, and the detailed dimensions are given under the caption for Fig. 9. The entire ground plane has been maintained on the bottom side, and the modified maple leaf-shaped patch is positioned above a substrate with a relative permittivity of 2.77. Conductive textile is used for radiating components because of its high conductivity with the combination of nickel + copper-plated and silver-coated nylon [46]. Several methods for bandwidth enhancement have been used to achieve an ultra-wide bandwidth, including the adoption of bioinspired radiating structures, etching slots, truncating edges, and introducing stubs in the feeds, as covered in paper [12]. Figures 10 and 11 illustrate the prototype of the fabricated antenna from various perspectives, including Fig. 10(a) front view, 10(b)

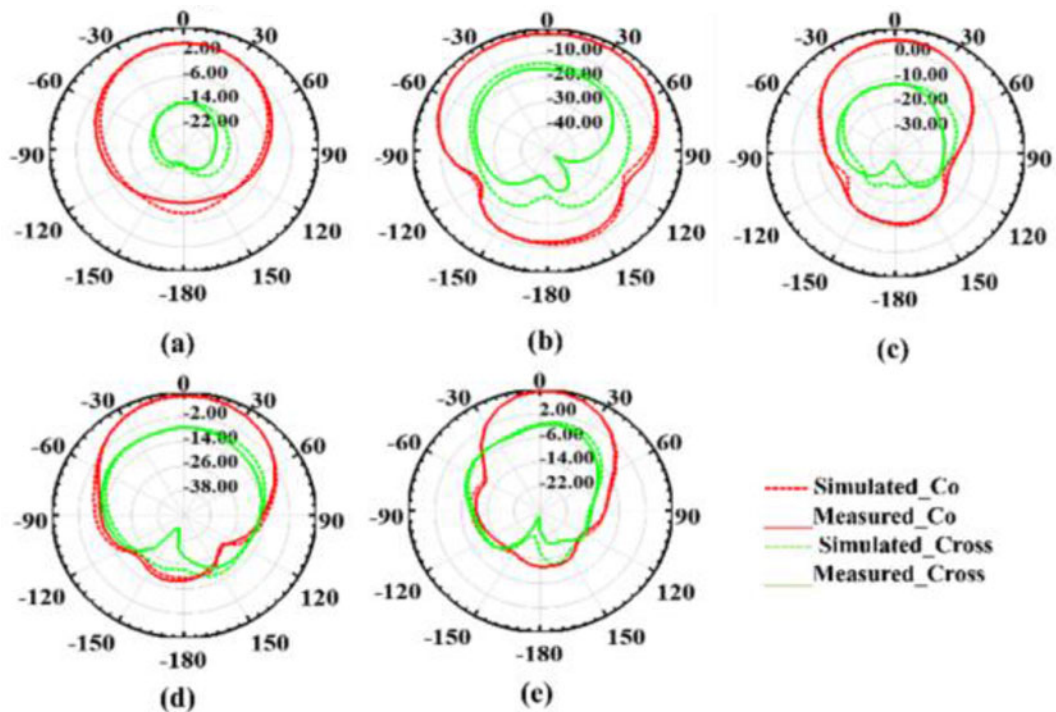


Figure 16. Simulated and measured E plane at various frequencies (a) 4.8 GHz, (b) 6.2 GHz, (c) 8.6 GHz, (d) 9.2 GHz and (e) 10.2 GHz.

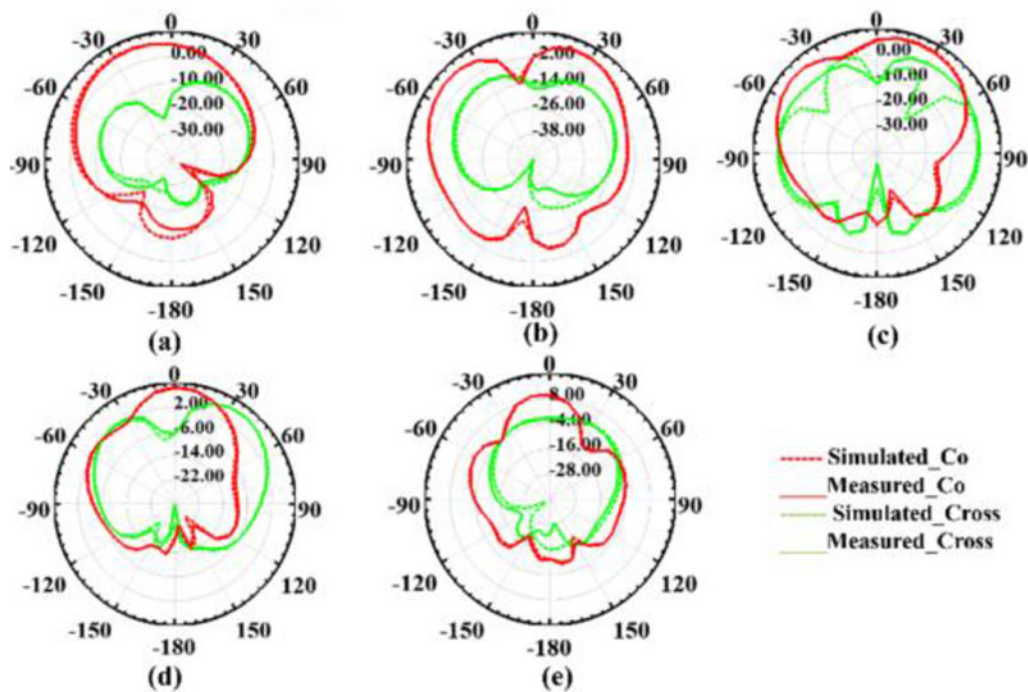


Figure 17. Simulated and measured H plane radiation pattern at (a) 4.8 GHz, (b) 6.2 GHz, (c) 8.6 GHz, (d) 9.2 GHz and (e) 10.2 GHz.

rear view, Fig. 11(a) X-bent, and 11(b) Y-bent, respectively. Surface current distribution diagrams at 3.1 GHz, 5.5 GHz, and 9.5 GHz frequencies covering lower, middle, and higher frequencies of the UWB band are shown in Fig. 12. From the surface current distribution, it is observed that the maximum current is at the feeding point and around the slot.

Experimental outcome

The performance of the proposed antenna is analyzed in free space and on body conditions. To test the flexibility, the MFG antenna is bent in X and Y orientations on a cylinder with a 30 mm radius. The on-body bending analysis is performed on a cylindrical dispersive

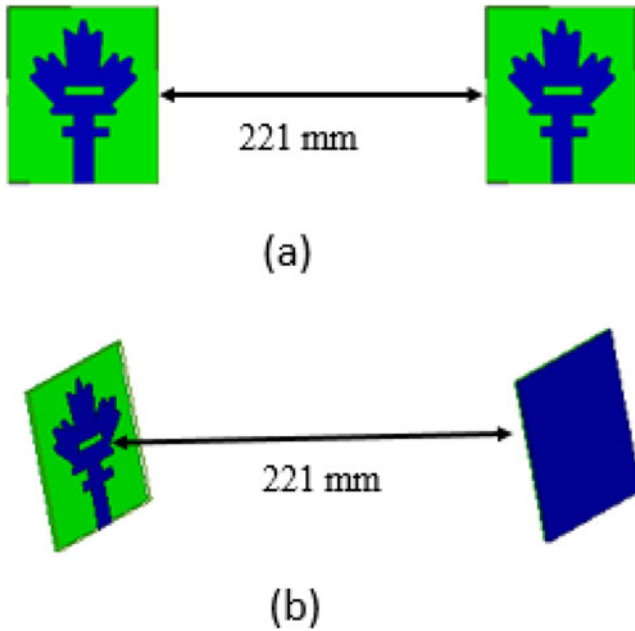


Figure 18. Antenna setup for group delay analysis (a) side by side (b) face to face.

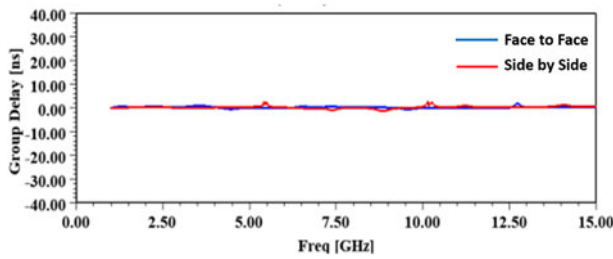


Figure 19. Group delay plot of the proposed MFG antenna.

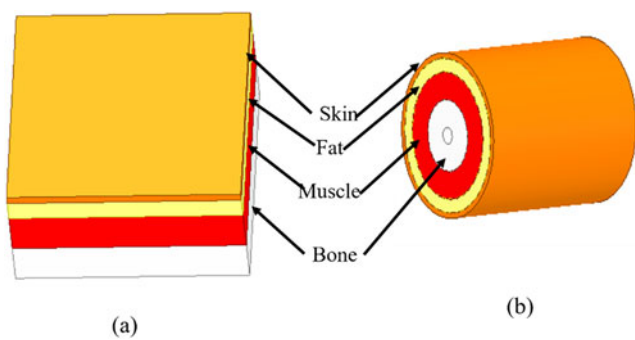


Figure 20. Human tissue layer model (a) flat (b) cylindrical.

human tissue model (HTM) of a 30 mm radius. To perform SAR analysis, the proposed antenna is placed on a flat human tissue layer model. Both the cylindrical dispersive HTM and flat human tissue layer model consisting of skin, fat, muscle, and bone with different dielectric constants values at different frequencies. The various layers of the human tissue model and corresponding dielectric properties at different frequencies are listed in Table 3 [47]. The antenna under test in the anechoic chamber is shown in Fig. 13.

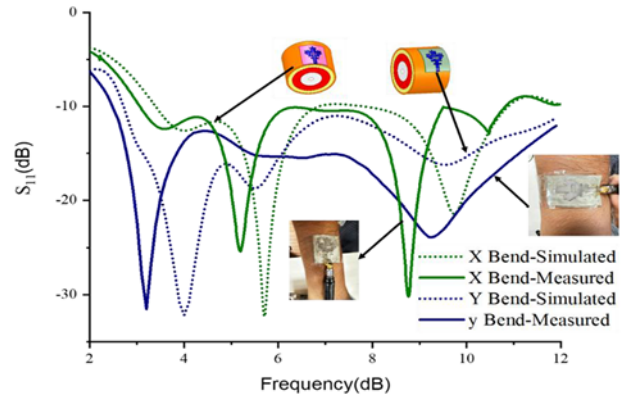


Figure 21. On body bending in X and Y orientations.

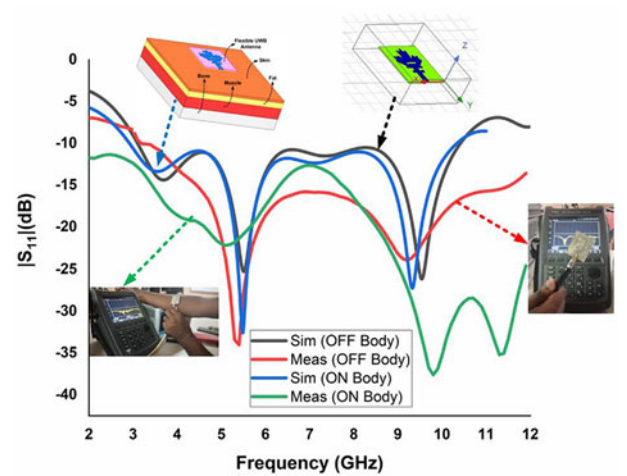


Figure 22. Return loss comparison of the simulated and measured return loss at 0 mm on flat human body model.

Free space measurements

The simulated and measured return loss in free space under flat and bent scenarios are compared in Figs. 14 and 15, respectively. The simulated return loss is identical to the measured in flat and bent conditions. It is noticeable that the measured results exhibited a wider bandwidth of 8.8 GHz, i.e., from 3.212 GHz. The E and H plane radiation patterns are measured in an anechoic chamber at different frequencies, such as 4.8 GHz, 6.2 GHz, 8.6 GHz, 9.2 GHz, and 10.2 GHz. Overall, as seen in Figs. 16–17, respectively, there is a noticeable agreement between the simulated and measurements at the E and H planes. As expected, the antenna mostly radiates in its boresight direction because of the complete ground plane. Consequently, this reduces the coupling between the antenna and the body, minimizing energy dissipation within the body and loading of the antenna.

Assessing the group delay of UWB antennas is crucial for verifying the undistorted nature of their structure. A consistent group delay signifies that the antenna is nonresonant, leading to effective radiation [48]. It is essential to minimize the group delay, with a maximum acceptable value of $Dt = 1/2$ fs, and for short pulse transmission, it should be 3.8 ns [49, 50]. Two identical antennas are positioned facing each other and in side-by-side orientations with far-field distance (D_s) of 221 mm calculating at 3 GHz frequency as shown in Fig. 18. The group plots are presented in Fig. 19,

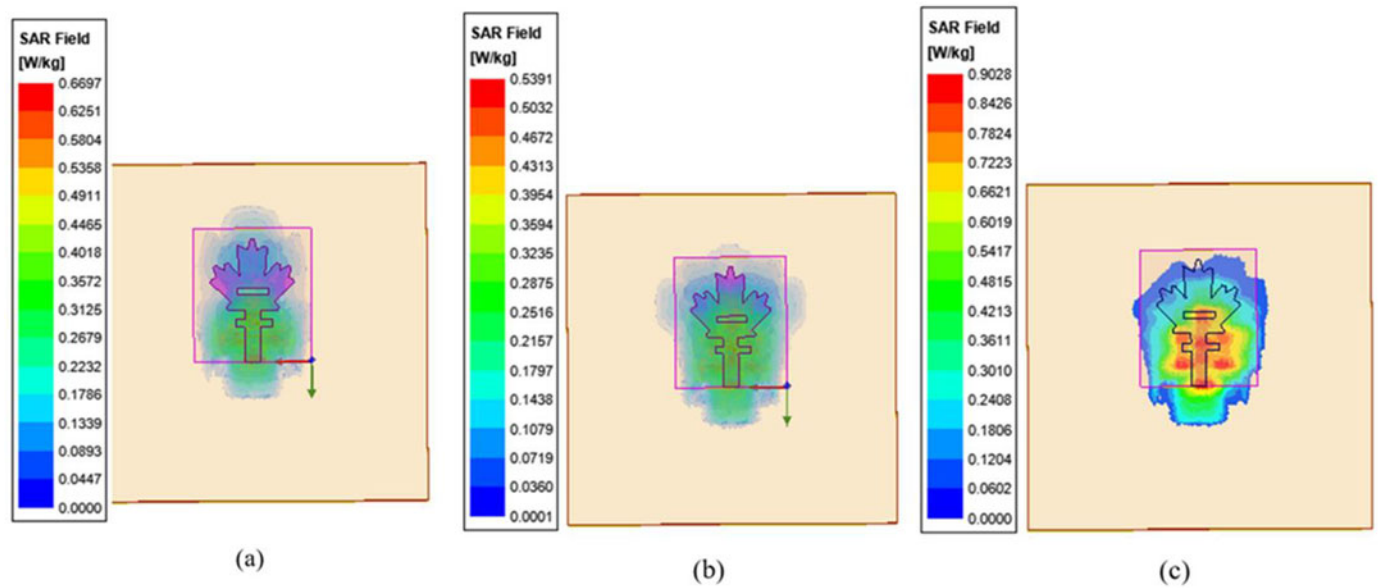


Figure 23. SAR values at (a) 3.8 GHz (b) 7.5 GHz and (c) 10 GHz.

Table 4. Comparison with state-of-art works

References	Size (mm ²)	Operating frequency (GHz)	Bandwidth (GHz)	Machine learning	Dielectric materials	Advantages/Limitations
[15]	80 × 61	3.1–10.6	7.5	No	All textile	Larger dimensions and complex-multi-layered structures, may not be watertight.
[22]	80 × 67	3.7–10.3	6.6	No	PDMS	Highly flexible, however, has larger dimensions and failed to cover the entire UWB range.
[28]	101 × 64	3.63–9.21	5.58	No	TacomcRF35	Larger dimensions and failed to cover the entire UWB range.
[27]	70 × 70	3.8–8.3	4.5	No	PDMS	Highly flexible, however, has larger dimensions and failed to cover the entire UWB range.
[51]	97 × 88	3.4–10.2	6.8	No	Felt	Larger dimensions and materials may not be water-tight
Proposed	35.5 × 30.5	3.1–10.42	7.32	Yes	PDMS	The smaller footprint is highly flexible due to the overall thickness of the antenna and covers the entire UWB range.

revealing that the variations are under 2.5 ns and exhibit an almost linear pattern across the entire UWB frequency range.

On-body measurements

It is essential to examine how the antenna affects the human body and vice versa to ensure the stability of the antenna's operation and the safety of human tissues. Using Ansys HFSS, a four-layered flat human body model and the cylindrical dispersive HTM are created, incorporating skin, fat, and muscle and bone as shown in Fig. 20. On-body bending analysis is performed both in X and Y orientations on a 30 mm radius cylindrical dispersive HTM. The corresponding return loss characteristics are compared and plotted in Fig. 21. From the plot it is evident that the antenna bent on the body in the X and Y axis agrees well maintaining the resonating bandwidth with negligible frequency shift. MFG antenna placed on the flat HTM (90 × 90 mm²) with 0 mm gap and comparison

of return loss is plotted in Fig. 22. It is observed that the proposed antenna exhibited $S_{11} < -10$ dB for 7.32 GHz bandwidth (3.1–10.42 GHz) over the human body for simulated results and bandwidth of 9.8 GHz (2.2–12 GHz) for measured results. The nonuniformity of the substrate is the reason for the discrepancies between the measured and simulated findings. The manufacturing fault that occurred during the soldering of the connection is another element that contributes to the mismatch. Mismatches have also been seen in the free space measurement facility since the proposed antenna input parameters were determined using a Vector Network Analyzer (VNA) in an open environment. Safety assessment involves measuring SAR, while antenna performance is evaluated through return loss measurements. As per the FCC standards, the maximum SAR limit is 1.6 W/kg for 1 g of tissue. The simulated SAR values for different frequencies with an input power of 25 mW are 0.66 W/kg, 0.53 W/kg, and 0.90 W/kg at 3.8 GHz, 7.5 GHz, and 10 GHz, respectively, as demonstrated in Fig. 23. It is

observed that the obtained SAR values are significantly lower than the FCC standards. The proposed antenna is compared with the state of artwork in Table 4. The comparison shows that the proposed antenna is a compact, single-layered structure with smaller dimensions covering the entire UWB.

Conclusion

This article presents a highly flexible UWB antenna for wearable applications. The dimensions of the proposed antenna are well-predicted and optimized using ML algorithms. The KNN ML algorithms accurately predict the S_{11} of the proposed antenna. The KNN ML algorithms give 99.62% compared to other ML algorithms. The ML algorithms are compared concerning training time, testing time, and accuracy. The proposed antenna has a compact footprint with a full ground plane. The MFG antenna exhibits a boresight radiation pattern as required in wearable applications. The proposed antenna maintains stable performance under flat, body, and bending conditions. The obtained SAR values are significantly lower than the FCC standards making it an ideal candidate for wearable applications.

Acknowledgements. The authors express gratitude to CSIR-NAL, Bangalore, for providing a facility to analyze the dielectric properties of the substrate material and to CABS, DRDO, Bangalore, for granting access to an anechoic chamber facility.

Author contributions. Conceptualization, methodology, software, investigation-PA, and JK.; resources, data curation-PA, and JK.; writing—original draft preparation, -PA and JK; writing—review and editing, -UG. and PR.; visualization, and Supervision-UG, and PR. All authors have read and agreed to the published version of the manuscript.

Funding statement. This research received no specific grant from any funding agency, commercial or not-for-profit sectors.

Competing interests. The authors report no conflict of interest.

References

1. Paracha KN, Rahim SK, Soh PJ and Khalily M (2019) Wearable antennas: A review of materials, structures, and innovative features for autonomous communication and sensing. *IEEE Access* 7, 56694–56712.
2. Lim HB, Baumann D and Li E (2011) A human body model for efficient numerical characterization of UWB signal propagation in wireless body area networks. *IEEE Transactions on Biomedical Engineering* 58(3), 689–697.
3. Mahmood SN, Ishak AJ, Ismail A, Zakaria Z and Alani S (2020) ON-OFF body ultra-wideband (UWB) antenna for wireless body area networks (WBAN): A review. *IEEE Access* 8, 150844–150863.
4. Yan S, Soh PJ and Vandenbosch GAE (2018) Wearable ultra-wideband technology—a review of ultra-wideband antennas, propagation channels, and applications in wireless body area networks. *IEEE Access* 6, 42177–42185.
5. Zhang K, Vandenbosch GAE and Yan S (2020) A novel design approach for compact wearable antennas based on metasurfaces. *IEEE Transactions on Biomedical Circuits and Systems* 14(4), 918–927.
6. Cavallari R, Martelli F, Rosini R, Buratti C and Verdone R (2014) A survey on wireless body area networks: Technologies and design challenges. *IEEE Communications Surveys and Tutorials* 16(3), 1635–1657.
7. IEEE Standard (2012) IEEE standard for local and metropolitan area networks—part 15.6: Wireless body area networks.
8. (2002) First order and report: Revision of part 15 of the commission's rules regarding UWB transmission systems.
9. Bahrami H, Mirbozorgi SA, Ameli R, Rusch LA and Gosselin B (2016) Flexible, polarization-diverse UWB antennas for implantable neural recording systems. *IEEE Transactions on Biomedical Circuits and Systems* 10(1), 38–48.
10. Andreu C, Castelló-Palacios S, Garcia-Pardo C, Fornes-Leal A and Cardona N (2016) Spatial in-body channel characterization using an accurate UWB phantom. *IEEE Transactions on Microwave Theory & Techniques* 64(11), 3995–4002.
11. Yeboah-Akokuwah B, Kosmas P and Chen Y (2017) A Q-slot monopole for UWB body-centric wireless communications. *IEEE Transactions on Antennas and Propagation* 65(10), 5069–5075.
12. Alomainy A, Sani A, Rahman A, Santas JG and Hao Y (2009) Transient characteristics of wearable antennas and radio propagation channels for ultrawideband body-centric wireless communications. *IEEE Transactions on Antennas and Propagation* 57(4), 875–884.
13. Abbasi QH, Rehman MU, Yang X, Alomainy A, Qaraqe K and Serpedin E (2013) Ultrawideband band-notched flexible antenna for wearable applications. *IEEE Antennas and Wireless Propagation Letters* 12, 1606–1609.
14. Bharadwaj R, Parini C and Alomainy A (2015) Experimental investigation of 3-D human body localization using wearable ultra-wideband antennas. *IEEE Transactions on Antennas and Propagation* 63(11), 5035–5044.
15. Yimdjopoffelie LA, Soh PJ, Yan S and Vandenbosch GAE (2016) A high-fidelity all-textile UWB antenna with low back radiation for off-body WBAN applications. *IEEE Transactions on Antennas and Propagation* 64(2), 757–760.
16. Sambandam P (2020) Compact monopole antenna backed with fork-slotted EBG for wearable applications. *IEEE Antennas and Wireless Propagation Letters* 19(2), 228–232.
17. Bharadwaj R, Alomainy A and Koul SK (2022) Experimental investigation of body-centric indoor localization using compact wearable antennas and machine learning algorithms. *IEEE Transactions on Antennas and Propagation* 70, 1344–1354.
18. Bharadwaj R, Swaisaenyakorn S, Parini C, Batchelor JC, Koul SK and Alomainy A (2020) UWB channel characterization for compact L-shape configurations for body-centric positioning applications. *IEEE Antennas and Wireless Propagation Letters* 19(1), 29–33.
19. Barakelobaid HA, Rahim SK, Himdi M, Castel X and Abe-Diankasgari M (2017) A transparent and flexible polymer-fabric tissue UWB antenna for future wireless networks. *IEEE Antennas and Wireless Propagation Letters* 16, 1333–1336.
20. Praveena A, Umamaheswari G and Sankar Ponnappalli VA (2023) Performance analysis of maple-shaped monopole multiband antenna on various substrate materials. *IETE Journal of Research* 69(3), 1233–1240.
21. Bakar AA, Hasnan F, Razali AR, Rahim AFA, Osman MS, Ali T and Radzali R (2019) Polydimethylsiloxane as a potential antenna substrate. *Acta Physica Polonica, A* 135(5), 1002–1004.
22. Simorangkir RBVB, Kiourti A and Esselle KP (2018) UWB wearable antenna with a full ground plane based on PDMS-embedded conductive fabric. *IEEE Antennas Wireless Propagation Letters* 17(3), 493–496.
23. Janapala DK, Nesusudha M and Neebha TM (2022) Design and Development of flexible PDMS antenna for UWB-WBAN applications. *Wireless Personal Communications* 122, 3467–3483.
24. Roy A, Biswas AK, Nandi A and Basu B (2023) Ultra-wideband flexible wearable antenna with notch characteristics for WLAN applications. *Progress in Electromagnetics Research C* 129, 143–155.
25. Chen P, Wang D and Gan Z (2023) Flexible and small textile antenna for UWB wireless body area network. *Micromachines* 14(4), 718.
26. Samal PB, Jammy Chen S and Fumeaux C (2023) Wearable textile multiband antenna for WBAN applications. *IEEE Transactions on Antennas and Propagation* 71(2), 1391–1402.
27. Mohamad Zade B, Simorangkir RB, Hashmi RM, Chao-Oger Y, Zhadobov M and Sauleau R (2019) A conformal band-notched ultrawideband antenna with monopole-like radiation characteristics. *IEEE Antennas and Wireless Propagation Letters* 19(1), 203–207.
28. Samal PB, Jack Soh P and Zakaria Z (2019) Compact microstrip-based textile antenna for 802.15. 6 WBAN-UWB with full ground plane. *International Journal of Antennas and Propagation*, 1–12.

29. Cao L (2022) A new age of AI: Features and futures. *IEEE Intelligent Systems* 37(1), 25–37.
30. Goudos SK, Diamantoulakis PD, Matin MA, Sarigiannidis P, Wan S and Karagiannidis GK (2022) Design of antennas through artificial intelligence: State of the art and challenges. *IEEE Communications Magazine* 60(12), 96–102.
31. Misilmani E, Hilal M, Naous T and Al Khatib SK (2020) A review on the design and optimization of antennas using machine learning algorithms and techniques. *International Journal of RF and Microwave Computer-Aided Engineering* 30(10), e22356.
32. Khan MM, Hossain S, Mozumdar P, Akter S and Ashique RH (2022) A review on machine learning and deep learning for various antenna design applications. *Heliyon* 8(4), e09317.
33. Shi D, Lian C, Cui K, Chen Y and Liu X (2022) An intelligent antenna synthesis method based on machine learning. *IEEE Transactions on Antennas and Propagation* 70(7), 4965–4976.
34. Ranjan P, Krishnan A, Dwivedi AK, Singh SK and Sharma A (2023) Design and optimization of MIMO dielectric resonator antenna using machine learning for sub-6 GHz based on 5G IoT applications". *Arabian Journal for Science and Engineering* 48, 1–9.
35. Rai JK, Ranjan P and Chowdhury R (2024) Machine learning enabled Al₂O₃ ceramic based dual band frequency reconfigurable dielectric antenna for wireless application. *IEEE Transactions on Dielectrics and Electrical Insulation*.
36. Dwivedi AK, Singh SK, Ranjan P, Sharma A and Singh V (2024) Machine learning assisted dual port metasurface loaded MIMO antenna with linearly polarized to circularly polarized conversion features for n257 band of 5G mm-wave applications. *International Journal of Communication Systems* 37(8), e5737.
37. Rai JK, Ranjan P and Chowdhury R (2024) Recent development in reconfigurable dielectric resonator antenna and microwave filter: Design and application. *International Journal of Communication Systems*, e5859.
38. Rai JK, Ranjan P, Chowdhury R and Jamaluddin MH (2024) Design and optimization of dual port dielectric resonator based frequency tunable MIMO antenna with machine learning approach for 5G new radio application. *International Journal of Communication Systems* 37, e5856.
39. Sharma Y, Zhang HH and Xin H (2020) Machine learning techniques for optimizing design of double T-shaped monopole antenna. *IEEE Transactions on Antennas and Propagation* 68(7), 5658–5663.
40. Ranjan P, Pandey S and Kumar Rai J (2022) Investigation of rectangular dielectric resonator antenna using machine learning optimization approach. In *2022 IEEE Conference on Interdisciplinary Approaches in Technology and Management for Social Innovation (IATMSI)*. IEEE.
41. Rai JK, Ranjan P and Chowdhury R (2023) Frequency reconfigurable wideband rectangular dielectric resonator antenna for sub-6 GHz applications with machine learning optimization. *AEU-International Journal of Electronics and Communications* 171, 154872.
42. Rai JK, Anuragi K, Mishra N, Chowdhury R, Kumar S and Ranjan P (2024) Dual-band miniaturized composite right left handed transmission line zor antenna for microwave communication with machine learning approach. *AEU-International Journal of Electronics and Communications* 176, 155120.
43. Zarrabi FB, Shire AM, Rahimi M and Gandji NP (2014) Ultra-wideband tapered patch antenna with fractal slots for dual notch application. *Microwave and Optical Technology Letters* 56(6), 1344–1348.
44. Rahimi M, Heydari S, Mansouri Z, Gandji NP and Zarrabi FB (2016) Investigation and design of an ultra-wideband fractal ring antenna for notch applications. *Microwave and Optical Technology Letters* 58(7), 1629–1634.
45. Poorgholam-Khanjari S, Hatami A and Zarrabi FB (2021) Compact antenna based on split ring resonator as high Q-factor antenna for liquid permittivity measurements. *Frequenz* 75(7-8), 275–287.
46. <https://protocentral.com/product/woven-conductive-fabric-silver-20cm-square>.
47. <http://niremf.ifac.cnr.it/tissprop/>.
48. Wiesbeck W, Adamiuk G and Sturm C (2009) Basic properties and design principles of UWB antennas. *Proceedings of the IEEE* 97 (2), 372–385.
49. Biswas RG and Poddar DR (2017) A fern fractal leaf inspired wideband antipodal Vivaldi antenna for microwave imaging system. *IEEE Transactions on Antennas and Propagation* 65(11), 6126–6129.
50. Narbudowicz A, John M, Sipal V, Bao X and Ammann MJ (2015) Design method for wideband circularly polarized slot antennas. *IEEE Transactions on Antennas and Propagation* 63(10), 4271–4279.
51. Samal PB, Soh PJ and Vandenbosch GAE (2014) UWB all-textile antenna with full ground plane for off-body WBAN communications. *IEEE Transactions on Antennas and Propagation* 62(1), 102–108.



Alladi Praveena is pursuing her PhD (under QIP) at PSG College of Technology, Coimbatore. She received her M. Tech (Embedded Systems) from Sreyas Institute of Engineering and Technology, Hyderabad in the year 2014. She is working as Assistant Professor in the department of Electronics and Communication Engineering, Sreyas Institute of Engineering and Technology. She has 6 years of teaching experience and her research interests include Communication Systems, Antenna Design, Artificial Intelligence and Machine learning. She is the member in IEEE.



Govindaswamy Umamaheswari completed her PhD in the area of Information Security from Bharathiar University in the year 2006. She is currently working as Associate Professor in the department of ECE, PSG College of Technology. She has 25 years of teaching experience and her research interests include Communication Systems, Wireless Networks and Wireless Security. She has published 65 papers in national and international journals and conferences. 10 research students have been awarded PhD. Degree in the field of Wireless Communications, Image processing and information security. She is the member in ISTE, IE, CRSI, and ISSS.



Jayant Kumar Rai was born in Kanker (Chhattisgarh), India, in 1990. He is working as a Lecturer (ET&T) at RKR Government Polytechnic, Janjgir Champa, Chhattisgarh. He received his B.E. degree in Electronics & Telecommunication Engineering in 2011 and MTech in E&TC (Communication) in 2016 from Chhattisgarh Swami Vivekanad Technical University (CSVТУ), BHILAI, (C.G.). He has more than 7 years of teaching/research experience. He is currently doing PhD under the QIP Scheme from ABV-Indian Institute of Information Technology and Management, Gwalior, Madhya Pradesh. He has authored or co-authored more than 25 research papers in international/national journals/Conference proceedings. His research interests include Dielectric Resonator Antenna, MIMO, Machine Learning, and Reconfigurable Antenna.



Pinku Ranjan, ABV IITM Gwalior, Madhya Pradesh, India. Presently he is working as an Assistant Professor in the Dept. of Electrical and Electronics Engineering, ABV-IITM Gwalior, M.P, India. He received his Ph.D with integrated M.Tech from the Department of Electronics Engineering, IIT (ISM) Dhanbad, Jharkhand, India in October 2017. He received his B. Tech in Electronics and Communication Engineering

from Jawaharlal Nehru Technological University (JNTU) Hyderabad, India, in 2010. He served as JRF/SRF in the Department of Electronics Engineering, IIT Dhanbad, India, from August 2012 to July 2017. He served as a Research Assistant Professor in the ECE Department at SRM IST Chennai from

June 2017 to March 2019. He has authored or co-authored more than 90 research papers in international/ national journal/conference proceedings. He is a reviewer of many international/ national journal/conference proceedings. His research interests include Dielectric Resonator Antenna, MIMO 5G Antenna, Monopole Antenna, multiband Hybrid Antennas, Circularly Polarized Antennas, Wearable Antenna, Bio- Electromagnetics, Machine Learning, Deep learning, IOT devices and Image processing, RIS, Metamaterial Bio-sensor, Reconfigurable antenna, Terahertz 6G antennas. He is an IEEE Senior member. Under his guidance more than 50 B.Tech and 30 M.Tech completed thesis work, 5 Ph.D working. He received 4 sponsored projects.